

First Steps Toward Translating Robotic Walking To Prostheses: A Nonlinear Optimization Based Control Approach

Huihua Zhao · Jonathan Horn · Jacob Reher · Victor Paredes · Aaron D. Ames

Received: date / Accepted: date

Abstract This paper presents the first steps toward successfully translating nonlinear real-time optimization based controllers from bipedal walking robots to a self-contained powered transfemoral prosthesis: AMPRO, with the goal of improving both the tracking performance and the energy efficiency of prostheses control. To achieve this goal, a novel optimization-based control strategy combining control Lyapunov function (CLF) based quadratic programs (QP) with impedance control is proposed. This optimization-based controller is first verified on a human-like bipedal robot platform, AMBER. The results indicate improved (compared to variable impedance control) tracking performance, stability and robustness to unknown disturbances. To translate this complete methodology to a prosthetic device with an amputee, we begin by collecting reference locomotion data from a healthy subject via Inertial measurement Units (IMUs). This data forms the basis for an optimization problem that generates virtual constraints, i.e., parameterized trajectories, specifically for the amputee. A online optimization based

Huihua Zhao
Mechanical Engineering, Georgia Institute of Technology
Atlanta, GA USA. E-mail: huihua@gatech.edu

Jonathan Horn
Mechanical Engineering, Texas A&M University
College Station, TX USA. E-mail: j.horn@tamu.edu

Jacob Reher
Mechanical Engineering, Georgia Institute of Technology
Atlanta, GA USA. E-mail: jpreher@gatech.edu

Victor Paredes
Mechanical Engineering, Texas A&M University
College Station, TX USA. E-mail: vcparedesc@tamu.edu

Aaron D. Ames
Mechanical Engineering, Georgia Institute of Technology
Atlanta, GA USA. E-mail: ames@gatech.edu

controller is utilized to optimally track the resulting desired trajectories. An autonomous, state based parameterization of the trajectories is implemented through a combination of on-board sensing coupled with IMU data, thereby linking the gait progression with the actions of the user. Importantly, the proposed control law displays remarkable tracking and improved energy efficiency, outperforming PD and impedance control strategies. This is demonstrated experimentally on the prosthesis AMPRO through the implementation of a holistic sensing, algorithm and control framework, resulting in dynamic and stable prosthetic walking with a transfemoral amputee.

Keywords Transfemoral prosthesis control · real-time optimal control · hybrid systems · quadratic program · optimization problem

1 INTRODUCTION

There are approximately 222,000 people in the United States alone that are transfemoral amputees [1]. Despite this large demographic, the current market for commercial transfemoral prostheses remains largely limited to energetically passive prosthetic devices, limiting the day-to-day life of amputees with increased metabolic cost and constrained locomotion capabilities [2]. As one of the most important applications of bipedal robotic research, powered lower-limb prostheses capable of providing net power in conjunction with various prostheses controllers have been developed in recent decades. Most notably, [3,4] developed a hydraulically actuated knee prosthesis with the “echo control” method to mirror the modified trajectory of a healthy leg to the opposing side. Gait-pattern generator based controllers have been successfully realized on prostheses [5,6]. An optimal design of a transfemoral prosthesis with energy storage and regeneration is presented in [7]. Control of a powered prosthetic leg through virtual constraints using the Center of Pressure (COP) as a phasing variable was realized in [8]. Under the assumption that the human gait is cyclic, variable impedance control is one of the most common approaches for controlling prostheses [9–14]. However, despite the improvements that these smart controllers have achieved, there are still limitations related to the optimality of the controllers and the need for exhaustive clinical testing to determine control parameters. These issues motivate the main objectives of this paper.

The primary goal of this paper is to demonstrate the successful translation of advanced controllers from robotic walking to prostheses, with the end result being improved energy efficiency given similar tracking performance compared to existing control strategies (PD and variable impedance control). In particular, the main contributions of this work are threefold: a) propose the idea of utilizing bipedal

robots to test a systematical method for prosthetic control, which includes a simple IMU data recording procedure, an automatic gait generation process and an optimization-based nonlinear controller. b) To introduce the custom designed self-contained powered transfemoral prosthetic device AMPRO explicitly with the goal to validate this systematic method on an amputee subject. c) To close the loop on the translation of bipedal locomotion to prosthetic walking via the implementation of the systematic methodology on an amputee while achieving stable and efficient walking on a powered prosthesis. Detailed context of the experiment framework and experimental results analysis are provided for discussion and verification.

A novel prosthetic controller that combines the rapidly exponentially stabilizing control Lyapunov functions (RES-CLFs) with impedance control is proposed with the goal of achieving better tracking and improved energy efficiency on prostheses. This controller was first verified in simulation [15] and then tested on a human-like bipedal robot platform: AMBER (Advanced Mechanical Bipedal Experimental Robot), which has been used in previous work [16] to achieve stable “prosthetic” walking. These successes on robotic systems motivate the realization of this controller on a custom-built prosthetic device: AMPRO. To begin, human walking trajectories are recorded through an Inertial Measurement Unit (IMU) motion capture system. With the collected data, a human-inspired optimization problem is then leveraged to obtain a stable gait which can be directly implemented for a specific test subject. IMUs are also used to estimate human movements during walking, thus providing human-robot sensory feedback.

Through the systematic methodology for translating human-inspired robotic walking to prostheses, stable and robust prosthetic walking is realized for an amputee subject, as shown in Fig. 1. The powered prosthetic walking gait is compared with the original walking gait of the amputee subject using a passive device, showing that the powered gait is natural and human-like. More importantly, the proposed controller also outperforms other existing controllers (such as PD) w.r.t. both better tracking (20.9% improvement on the e_{rms}) and improved power consumption (9.4% reduction). To summarize, the procedure for testing this controller both in simulation and on the bipedal robot helped to predict and resolve many implementation issues before attempting to realize walking with a human test subject. The presented procedure, therefore, has the potential to reduce the cost of clinical testing of prostheses through the fast and efficient development and testing of controllers.

The structure of this paper is as follows: In Sec. 2, the overall process for obtaining an optimized set of trajectories specific to AMPRO and the subject is outlined. This process begins with the collection of a nominal set of locomotion data which is then used as a seed in a human-inspired optimi-

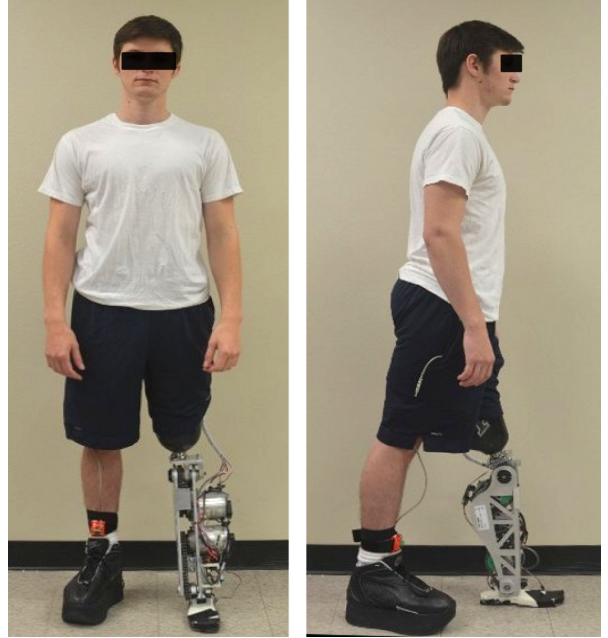


Fig. 1: Transfemoral test subject wearing the custom built prosthetic device, AMPRO (Advanced Mechanical Prosthetic).

mization to obtain the optimized trajectories for the prosthesis. Unifying RES-CLFs based quadratic programming control and the impedance control, the novel *model independent quadratic program* (MIQP) controller is discussed explicitly in Sec. 3. Before the implementation on the actual prosthetic device, the systematic methodology, including gait generation and optimization-based control, is verified in both simulation and experiment with the bipedal robot AMBER in Sec. 4. Finally, the experimental realization of the nonlinear online optimization based controller on a real prosthetic device with an amputee test subject is illustrated in Sec. 5. Conclusions and future work are presented at the end.

2 ROBOTIC MODEL OF HUMAN LOCOMOTION

In an effort to achieve human-like robotic walking, we turn to the most prevalent source—the human body—for natural and efficient locomotion. In particular, a low-cost inertial motion capture system with IMUs is developed and interfaced with the human-inspired control approach. This system is first used to capture the walking trajectories of a human subject. Utilizing the collected human locomotion data as the reference, an optimization problem is employed to design a stable (theoretically sound) and optimal (w.r.t torque, foot clearance, joint position and velocity) gait which can be directly implemented on the specific robot or test subject.

2.1 Motion Capture with IMU

There have been many methods proposed for ambulatory measurement of human joint angles. In particular, Luinge and Veltink [17] proposed a Kalman filter which integrates the 3D angular velocity while applying heading corrections based on accelerometer readings. This approach is prone to integration drift of the gyroscope for systems which need to operate for long durations of time such as prostheses. A more advanced kinematic filtering method was proposed by Roetenberg et al. [18] for the XSens MVN motion capture suit. This approach uses a kinematic model of the individual body segments which is used to update a Kalman filter and provide the positions of each joint and segment of the body. Motion capture systems have also been shown to be effective for robotic teleoperation such as the method proposed by Miller et al. [19] in which an inertial motion capture system was successfully used to teleoperate the NASA Robonaut. This system used a complementary filter to fuse accelerometers, gyroscopes, and magnetometers to estimate poses which were then used to compute an inverse kinematic relationship for pose recreation on the robot.

The algorithm used for motion capture in this work is a planar modification of the model-based EKF first presented by Šljajpah et al. [20]. In this approach, the human extremities are modeled as a kinematic chain built from a location of negligible acceleration. The concept is based on a kinematic relation similar to a series of inverted pendula, where the acceleration of any point B on a rigid body can be determined if the angular velocity, angular acceleration and linear acceleration of other point A on the body are known through the relation:

$$\mathbf{a}_B = \mathbf{a}_A + \boldsymbol{\omega} \times (\boldsymbol{\omega} \times \mathbf{r}_{AB}) + \dot{\boldsymbol{\omega}} \times \mathbf{r}_{AB}, \quad (1)$$

where \mathbf{r}_{AB} is the distance from point A to point B and $\boldsymbol{\omega}$ is the angular velocity of the link. The algorithm used in this work is different in two aspects: the kinematic model of the human legs is assumed to be composed of joints with ranges of motion limited to flexion/extension, and the kinematic chain is built from the hip. Since AMPRO has restricted actuation in solely the sagittal plane and because joint variations in the coronal plane are not used in the proposed control approach, only measurements resulting in joint flexion and extension are used in the model update. To express the segment estimation in terms of the available joint mobility of AMPRO, the measurements from the IMUs are projected onto the sagittal plane at each time step before they are passed to the filter. Additionally, we assume that the forward velocity of the hip is constant [21], [22] and that sinusoidal movement of the hip in the vertical direction will yield negligible acceleration in comparison to walking dynamics.

An EKF is instantiated for each segment in the model and updated sequentially along the kinematic chain from the

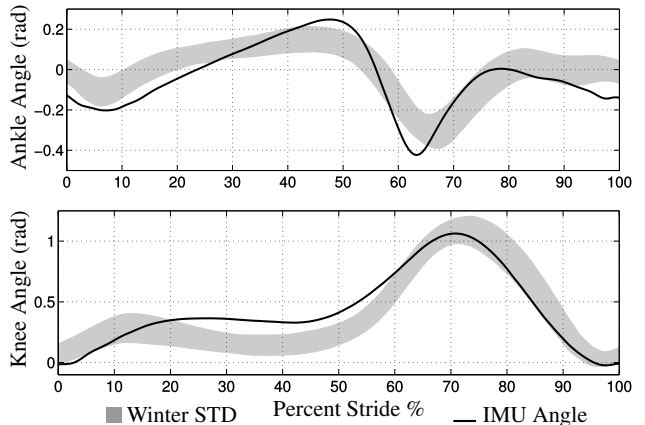


Fig. 2: Average joint angles for human subject using EKF filter as compared to Winter [23]. The trajectories are used as a comparison to show that the subject is walking with qualitatively humanlike trajectories for use in the trajectory optimization.

hip. More specifically, the hip joint is instantiated as a base in which the acceleration and angular velocity are zero. Each distal joint in the chain is then treated as a moving base, where the base acceleration and angular velocity are provided by the previous link. Each EKF update estimates the states $x_k = [\boldsymbol{\omega}^S, \dot{\boldsymbol{\omega}}^S, q^E, \dot{q}^E]^T$, with $\dot{\boldsymbol{\omega}}^S$ the first time derivative of the angular velocity in the segment (S) frame and \dot{q}^E the first time derivative of the earth-frame (E) quaternion. The measurements for each link are $z_k = [\boldsymbol{\omega}_k^S, \dot{\boldsymbol{\omega}}_k^S, \mathbf{a}_k^S]$ with \mathbf{a}_k^S the linear acceleration of the link, which is the primary measurement coupled to the previous link. Specifically, the acceleration from the previous joint is used in the estimation model as (1) where a_B is the expected accelerometer reading, and a_A is passed from the previous link. The estimation then proceeds through each joint according to the method detailed in [20].

Finally, the estimated orientations from the multibody EKFs are then used to extract the joint configuration using each link's quaternion attitude in the global frame ${}^E q$, from which the joint rotations used in the overall model q_j can be found as:

$$q_j = q_P^* \otimes q_D, \quad (2)$$

where q_P^* denotes the quaternion conjugate, \otimes is the quaternion product, q_D is the distal segment orientation and q_P is the proximal segment orientation.

During the experiment, the subject was asked to walk along a straight line for several steps while wearing seven IMUs to capture the walking behavior of the feet, shanks, thighs, and torso. The joint states are estimated and collected with the EKF algorithm. Then the joint angles are calculated by converting the joint rotation found in (2) to an Euler angle representation. Finally, several steps are averaged to yield their unique trajectories for optimization. While a thorough

investigation on the accuracy of the 3D estimation method was performed by Šlajpah et al., a comparison of the walking captured via the 2D projection was not validated with an optical tracking system. To verify that the EKF method is qualitatively capturing the human motion, knee and ankle joint angles of a healthy subject are compared to a standard set of sagittal plane gait kinematics findings by Winter [23] as shown in Fig. 2.

2.2 Robot Model.

A 7-link planar bipedal robot (one torso, two thighs, two calves and two feet) with anthropomorphic parameters corresponding to the test subject is considered as the robotic model of a human in this work. Due to the existence of discrete behavior present in walking, i.e., impacts due to foot strike, we represent the bipedal robot as a hybrid system [24] with the configuration space Q_R : $\theta = (\theta_{sa}, \theta_{sk}, \theta_{sh}, \theta_{nsh}, \theta_{nsk}, \theta_{nsa})^T$ as shown in Fig. 3. The equations of motion of the continuous dynamics are derived using the Euler-Lagrange formula:

$$D(\theta)\ddot{\theta} + H(\theta, \dot{\theta}) = Bu, \quad (3)$$

where $D(\theta) \in \mathbb{R}^{6 \times 6}$ is the inertial matrix and $H(\theta, \dot{\theta}) = C(\theta, \dot{\theta})\dot{\theta} + G(\theta) \in \mathbb{R}^{6 \times 1}$ contains the terms resulting from the Coriolis effect, centrifugal forces and the gravity vector. $B = I_6$ is the torque map and u is the vector of torque inputs. With the notation $x = (\theta; \dot{\theta})$, the affine control system $\dot{x} = f(x) + g(x)u$ can be obtained by reformulating (3) [25]. The discrete behavior of impact is modeled with the perfectly plastic impact assumption, i.e., there is no deformation, slippage or bounce during the impacts. This is a common practice in robotic modeling literature; more details can be found in [26–28].

Human-Inspired Outputs. With the goal of characterizing human locomotion, we take the perspective of viewing the “complex” human locomotion system as a “black box”. The goal of designing human-like trajectories for robots or prostheses then becomes to drive the actual robot outputs $y^a(\theta)$ to the desired human outputs $y^d(t, \alpha)$ which can be represented by the canonical walking function (CWF) and parameterized by a set α as:

$$y_{cwf}(t, \alpha) = e^{-\alpha_4 t} (\alpha_1 \cos(\alpha_2 t) + \alpha_3 \sin(\alpha_2 t)) + \alpha_5. \quad (4)$$

This function has been shown to be able to characterize human motion primitives universally including walking, running and stair climbing in previous work [26, 21]. For the pinned 7-link bipedal robot model considered in this paper, a total of 6 outputs are of interest including forward hip velocity (*hip*), knee angles (*sk*, *nsk*), non-stance slope (*nsl*),

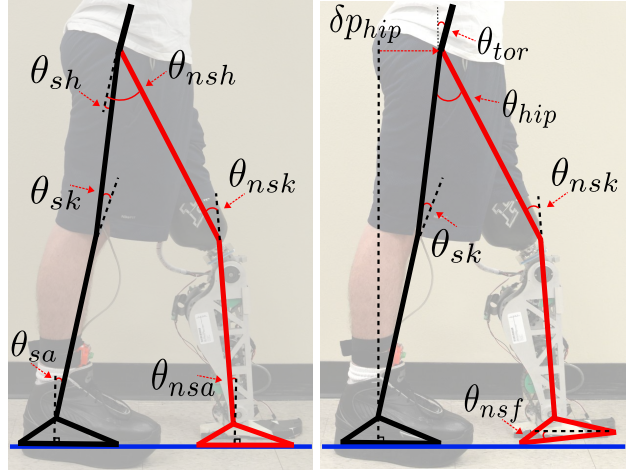


Fig. 3: Coordinates (left) and outputs configuration (right) of the flat-foot prosthetic model.

torso angle (*tor*) and non-stance foot angle (*nsf*) as in Fig. 3. Therefore, we introduce the human-inspired outputs:

$$y(\theta, \dot{\theta}, \alpha) = \begin{bmatrix} y_1(\theta, \dot{\theta}, \alpha) \\ y_2(\theta, \alpha) \end{bmatrix} = \begin{bmatrix} y_1^a(\theta, \dot{\theta}) - v_{hip} \\ y_2^a(\theta) - y_2^d(\rho(\theta), \alpha) \end{bmatrix}, \quad (5)$$

where $y_1(\theta, \dot{\theta}) = y_1^a(\theta, \dot{\theta}) - v_{hip}$ is the difference between the actual and desired hip velocity, and relative degree two outputs $y_2(\theta, \alpha) = y_2^a(\theta) - y_2^d(\rho(\theta), \alpha)$ contain the differences between the actual and desired relative degree two outputs. Note that, the desired relative degree two outputs are defined as $y_2^d(\rho(\theta), \alpha) = [y_{cwf}(\rho(\theta), \alpha_i)]_{i \in O}$ with $\alpha_i = (\alpha_{i,1}, \alpha_{i,2}, \alpha_{i,3}, \alpha_{i,4}, \alpha_{i,5})$ in (4), and $O = \{sk, nsk, nsl, tor, nsf\}$ is the set of relative degree two outputs. The parameters of all of the outputs are then combined to yield a single vector $\alpha = (v_{hip}, \alpha_{sk}, \alpha_{nsk}, \alpha_{nsl}, \alpha_{tor}, \alpha_{nsf}) \in \mathbb{R}^{26}$.

Upon observation of human locomotion data, the linearized forward hip position, $\delta p_{hip}(\theta)$, was discovered to increase linearly through the progress of a step cycle [21], [22], [29], therefore, motivating the phase variable:

$$\rho(\theta) = (\delta p_{hip}(\theta) - \delta p_{hip}^+)/v_{hip}, \quad (6)$$

which is used to parameterize a given walking gait as indicated in the formula of the desired outputs. Note that, the initial forward hip position $\delta p_{hip}^+(\theta)$ will be decided through the gait optimization which will be discussed later.

2.3 Human-Inspired Optimization

Using these outputs, a feedback linearizing controller [26] with a sufficiently large gain can be used to ensure that $y_2 \rightarrow 0$ for all time. If this condition is satisfied then the system is said to be on the partial zero dynamics surface,

$$\mathbf{PZ}_\alpha = \{(\theta, \dot{\theta}) \in T Q_R : y_2(\theta, \alpha) = \mathbf{0}, L_f y_2(\theta, \alpha) = \mathbf{0}\}, \quad (7)$$

This surface will be rendered invariant through the control law over the continuous dynamics; however, no guarantees can be made on invariance through discrete impacts in the system. As a result, the optimization parameters α of the outputs must be chosen in a way which renders \mathbf{PZ}_α invariant through impact, i.e., which yield partial hybrid zero dynamics surface (PHZD). These constraints can be explicitly stated as:

$$\Delta_R(S_R \cap \mathbf{PZ}_\alpha) \subseteq \mathbf{PZ}_\alpha, \quad (\text{PHZD})$$

where Δ_R and S_R are the reset map and switching surface of the robot model, respectively. The detailed explanation of these constraints can be found in [26].

By enforcing the PHZD constraints discussed above, the human-inspired optimization can be used to generate robot or prosthetic trajectories that are both provably stable and human-like [26]. More importantly, for a lower-limb prosthesis interacting with humans in a safety critical fashion, more attention must be placed on the physical constraints that relate to safety and energy conservation. One particular goal, for example, is to optimize the torque profile such that it is within the limit of the motors in order to bear the human weight during the stance phase. Walking gaits which require reduced torques also tend to decrease the energy consumption of the device, prolonging battery life. These specifications yield the optimization problem subject to both the PHZD constraints and physical constraints as stated in the following:

$$\begin{aligned} \alpha^* = \underset{\alpha \in \mathbb{R}^{26}}{\operatorname{argmin}} \operatorname{Cost}_{\text{HD}}(\alpha) \\ \text{s.t } \text{PHZD Constraints,} \\ \text{Physical Constraints,} \end{aligned} \quad (\text{HIO})$$

where the cost function of (HIO) is the least-square-fit error between the human experimental data (discussed in Sec. 2.1) and the CWF representations (5). The explicit expression of the cost function is stated as follows:

$$\operatorname{Cost}_{\text{HD}}(\alpha) = \sum_{i \in O} \sum_{k=1}^{K_i} \left(y_i^a[k] - y_i^d(t_i^a[k], \alpha_i) \right)^2, \quad (8)$$

where t_i^a and K_i are the discrete time and the number of discrete points for the recorded output $i \in O$, respectively.

Note that the physical constraints also include additional constraints such as foot clearance and limitations on actuator range of motion. The direct result of this optimization problem is the parameter set α that renders an optimal (w.r.t. torque, foot clearance, joint position and velocity) and provably stable human-like walking gait (which can be tested and verified in simulation). In particular, the term of stability mentioned here is specific to the mathematical stability of the designed gait, i.e., the gait has a limit cycle that is exponentially stable [24]. While this stability property does

not guarantee stable experimental walking (w.r.t the walking balance) of the prosthetic device, it plays a key role for testing and verifying prosthetic controllers on the bipedal robots in both simulation and experiment before implementing on prosthetic device. Additionally, due to the satisfaction of embedded hardware constraints, the gait can be directly implemented on the robot or prosthetic device.

To summarize, this optimization problem uses the trajectory of a healthy subject as the reference, which is subject to PHZD constraints (to ensure smooth transitions between stance and swing phase) and physical constraints (torque and angle limitations) such that the output gait is applicable for implementation on the prosthetic device. Therefore, the main advantages of utilizing this optimization problem are twofold: a) a smooth gait can be designed for a specific amputee without hand tuning and, b) the output gait can be used directly on the prosthetic device with reduced torque and improved energy efficiency.

Remark. The main goal of this research is to translate robotic walking into the design and control of prostheses aiming to achieve potentially reduced clinical tuning and improved energy performance. Utilizing the (HIO) optimization problem, a formally stable prosthetic gait can be generated automatically. While the optimized gait is a local minimal, the optimization problem can be easily re-performed with new constraints or feedbacks from the user. For example, the initial gait which was designed for this work included more stance knee movement, i.e., the stance knee angle was more human-like with more pronounced knee bend through the stance phase. During experiments, the test subject voiced that they would prefer a gait with less knee movement in this phase as it would feel safer to them. This preference was easily added into the optimization, with the end result of a new gait which the subject liked more. These preliminary tests indicate that through the utilization of the proposed method, adaptation to user preferences can be stated in a mathematically intuitive way and the tuning of parameters can be potentially be reduced.

2.4 Prosthetic Trajectory Reconstruction

The result of the optimization problem (HIO) is the parameter set α that defines the human-inspired outputs. Via these outputs, we can obtain desired joint angles and angular velocities for the robot in every iteration through the inverse projection from the PHZD surface. This is achieved through a methodology termed the *PHZD reconstruction* [30]. In particular, on the PHZD surface, the zero dynamic coordinates can be defined as:

$$\xi_1 = \delta p_{\text{hip}}(\theta) := c\theta, \quad (9)$$

$$\xi_2 = y_1^a(\theta, \dot{\theta}) := \delta \dot{p}_{\text{hip}}(\theta) := c\dot{\theta}, \quad (10)$$

where c is the coefficient array defining the linearized hip position $\delta p_{\text{hip}}(\theta)$ [31]. As the direct result of (6) and (9), the desired relative degree two outputs can be stated as $y_2^d(\rho(\theta), \alpha) = y_2^d(\xi_1, \alpha)$. Similarly, due to the linearity of the actual relative degree two outputs, we have $y_2^a = H\theta$ and $\dot{y}_2^a = H\dot{\theta}$. Therefore, utilizing the fact that the actual outputs are equal to the desired outputs on the PHZD surface, we have the following relationships between the desired joints states and the desired outputs of the robot, which are given by:

$$\begin{aligned}\theta_d(\xi) &= \Psi(\xi_1, \alpha) = \begin{bmatrix} c \\ H \end{bmatrix}^{-1} \begin{pmatrix} \xi_1 \\ y_2^d(\xi_1, \alpha) \end{pmatrix}, \\ \dot{\theta}_d(\xi) &= \Phi(\xi_1, \xi_2, \alpha) = \begin{bmatrix} c \\ H \end{bmatrix}^{-1} \begin{pmatrix} v_{\text{hip}} \\ \frac{\partial y_2^d(\xi_1, \alpha)}{\partial \xi_1} \xi_2 \end{pmatrix}.\end{aligned}\quad (11)$$

The immediate result of this expression is that by knowing ξ_1 and ξ_2 (which are the linearized forward hip position and forward hip velocity, respectively), the desired angles and velocities can be obtained directly using the parameter α .

3 PROSTHETIC CONTROLLER DESIGN

This section will begin by briefly introducing the framework of variable impedance control. This traditional control approach is utilized in the development of a novel *control Lyapunov function* (CLF) [32] based *model independent quadratic program* (MIQP) controller for prosthetic joints.

3.1 Impedance Control for Prostheses

Based on the notion of impedance control in [33], the torque at each joint during a single step can be represented in a piecewise fashion by a series of passive impedance functions [10] of the form:

$$\mu^{imp} = k(\theta - q^e) + b\dot{\theta}, \quad (12)$$

where, k , q^e and b represent the impedance parameters for stiffness, equilibrium angle and damping, respectively, which are constant for a specific phase.

While impedance control with a finite state machine is one of the most widely used algorithms suggested to date [13, 10], one main challenge is that it requires the choice of the control parameters for each phase. Currently, clinicians and prosthetic researchers often choose these parameters by trial and error hand tuning for each patient as noted in [10]. Motivated by this shortcoming, the authors took a different approach in the previous work [34] to learn the impedance parameters for a lower-limb prosthesis by the observation of unimpaired human walkers. The results have been validated in both simulation and experiment with a transfemoral prosthetic device. As an extension of this work, it is also shown

that the impedance parameters can be estimated by using the least-square-error method to fit the simulated data or experimental data with the piecewise impedance functions. Therefore, by using the impedance estimation algorithm as discussed in the previous works, the impedance controller can be implemented directly on the robot or prosthetic device with minimal tuning [15, 16].

3.2 CLF Model Independent QP

As a means for stabilizing systems undergoing impacts, rapidly exponentially stabilizing control Lyapunov functions (R-ES-CLFs) were introduced in [32] to yield controllers with stronger convergence guarantees. Quadratic programs can be used to realize RES-CLFs via inequality constraints. When combined with impedance control (implemented as a feed-forward term), the result is a novel feedback prosthetic control methodology: Model Independent Quadratic Programs (MIQP)+Impedance control.

3.2.1 Human-Inspired Control Revisited

With the human-inspired outputs defined in (5), the dynamics in (3) can be reformulated as:

$$\begin{bmatrix} \dot{y}_1 \\ \ddot{y}_2 \end{bmatrix} = \underbrace{\begin{bmatrix} L_f y_1(\theta, \dot{\theta}) \\ L_f^2 y_2(\theta, \dot{\theta}) \end{bmatrix}}_{L_f} + \underbrace{\begin{bmatrix} L_g y_1(\theta, \dot{\theta}) \\ L_g L_f y_2(\theta, \dot{\theta}) \end{bmatrix}}_A u, \quad (13)$$

where L_f is the *Lie* derivative and A is the dynamic decoupling matrix, which is invertible because of the specific criterion of the outputs selection [16]. By picking $u = A^{-1}(-L_f + \mu)$, equation (13) becomes:

$$\begin{bmatrix} \dot{y}_1 \\ \ddot{y}_2 \end{bmatrix} = \mu. \quad (14)$$

By designing μ properly (see [26]) one can drive both $y_1 \rightarrow 0$ and $y_2 \rightarrow 0$ exponentially. However, due to the lack of model information, it is not possible to realize this controller on prostheses. As a result, traditional PID control or variable impedance control are typically seen as a more favorable option since it does not require model information and can be applied in a decentralized way. However, PID controllers (same as impedance controllers) lack formal guarantees (when applied to nonlinear systems) and require hand tuning [35]. This motivates the need to find a new control strategy that overcomes the weaknesses of PID control while maintaining model insensitivity.

3.2.2 CLF MIQP

By defining the vector $\eta = (y, \dot{y}) \in \mathbb{R}^{n_1+2 \times n_2}$ with n_1, n_2 denoting the numbers of relative degree one outputs and relative degree two outputs, respectively, equation (14) can be written as a linear affine control system:

$$\dot{\eta} = \underbrace{\begin{bmatrix} 0_{n_1 \times n_1} & 0_{n_1 \times n_2} & 0_{n_1 \times n_2} \\ 0_{n_2 \times n_1} & 0_{n_2 \times n_2} & I_{n_2 \times n_2} \\ 0_{n_2 \times n_1} & 0_{n_2 \times n_2} & 0_{n_2 \times n_2} \end{bmatrix}}_F \eta + \underbrace{\begin{bmatrix} I_{n_1 \times n_1} & 0_{n_1 \times n_2} \\ 0_{n_2 \times n_1} & 0_{n_2 \times n_2} \\ 0_{n_2 \times n_1} & I_{n_2 \times n_2} \end{bmatrix}}_G \mu. \quad (15)$$

Considering the Continuous Algebraic Riccati Equations (CARE) with $P = P^T > 0$:

$$F^T P + PF - PGG^T P + I = 0, \quad (16)$$

we can obtain the optimal solution $\mu = -G^T P \eta$. The solutions of the CARE also allows for the construction of a *rapidly exponentially stabilizing control Lyapunov function (RES-CLF)* [36]. By defining $\eta_\varepsilon = (y_p/\varepsilon; \dot{y}_p)$ with convergence rate $\varepsilon > 0$, we define the positive definite RES-CLF with respect to linear system (15) to be:

$$V_\varepsilon(\eta) = \eta^T \begin{bmatrix} \frac{1}{\varepsilon} I & 0 \\ 0 & I \end{bmatrix} P \begin{bmatrix} \frac{1}{\varepsilon} I & 0 \\ 0 & I \end{bmatrix} \eta := \eta^T P_\varepsilon \eta. \quad (17)$$

Differentiating this function yields:

$$\dot{V}_\varepsilon(\eta) = L_F V_\varepsilon(\eta) + L_G V_\varepsilon(\eta) \mu, \quad (18)$$

where $L_F V_\varepsilon(\eta) = \eta^T (F^T P_\varepsilon + P_\varepsilon F) \eta$, $L_G V_\varepsilon(\eta) = 2\eta^T P_\varepsilon G$.

In order to exponentially stabilize the system, we want to find μ such that, for a specifically chosen $\gamma > 0$ [32], we have:

$$L_F V_\varepsilon(\eta) + L_G V_\varepsilon(\eta) \mu \leq -\frac{\gamma}{\varepsilon} V_\varepsilon(\eta). \quad (19)$$

Therefore, a locally optimal μ could be found by solving the following quadratic program (QP):

$$m(\eta) = \underset{\mu \in \mathbb{R}^{n_1+n_2}}{\operatorname{argmin}} \mu^T \mu \quad (20)$$

$$\text{s.t. } \varphi_0(\eta) + \varphi_1(\eta) \mu \leq 0, \quad (\text{CLF})$$

where $\varphi_0(\eta) = L_F V_\varepsilon(\eta) + \frac{\gamma}{\varepsilon} V_\varepsilon(\eta)$ and $\varphi_1(\eta) = L_G V_\varepsilon(\eta)$. The end result of solving the QP problem is a piecewise locally optimal control input μ which is independent of model information, i.e., we obtain a MIQP. More explicitly, the main principle of the MIQP algorithm is to construct a linear control system (15) that only focuses on the errors between the actual outputs and desired outputs, while not requiring any information about the original model. Note that, in order to obtain admissible control inputs that are also subject to other constraints (for example, torque bounds due

to hardware limits), we relax the CLF constraints with a penalty value $p > 0$ [24]. In particular, we consider the MIQP:

$$\underset{(\delta, \mu) \in \mathbb{R}^{n_1+n_2+1}}{\operatorname{argmin}} p\delta^2 + \mu^T \mu \quad (21)$$

$$\text{s.t. } \varphi_0(\eta) + \varphi_1(\eta) \mu \leq \delta, \quad (\text{CLF})$$

$$\mu \leq \mu_{MAX}, \quad (\text{Max Torque})$$

$$-\mu \leq \mu_{MIN}. \quad (\text{Min Torque})$$

This QP problem yields the control input μ that regulates the errors of the output dynamics in a rapidly exponentially stable fashion while simultaneously guaranteeing the resulting torque is physically applicable. Note that, the control system (15) can also be considered as the affine form of the simplest trajectory tracking problem with $\dot{y} = \mu$. Therefore, the controller discussed in this section can potentially be implemented on a more general spectrum.

3.3 MIQP+Impedance Control

While MIQP control methods benefit from model independence, torque solutions are not necessarily unique (i.e. the controller will generate an identical torque for two systems with the same tracking error). Consequently, the controller will be less responsive to the actual system and will tend to have problems with overshoot. Therefore, model information is added in the form of impedance controllers to achieve a more responsive system; this motivates the introduction of MIQP+Impedance control. With the impedance controller μ^{imp} as a feed-forward term, the desired torque μ^d of the prosthetic joints can be stated as:

$$\mu^d = \mu^{qp} + \mu^{imp}, \quad (22)$$

where μ^{qp} is the torque computed from the MIQP problem. Taking this idea further, we add the impedance term μ^{imp} into the MIQP construction for the total hardware torque bounds, which yields the following MIQP+Impedance formula as follows:

$$\underset{(\delta, \mu^{qp}) \in \mathbb{R}^{n_1+n_2+1}}{\operatorname{argmin}} p\delta^2 + \mu^{qpT} \mu^{qp} \quad (23)$$

$$\text{s.t. } \varphi_0(\eta) + \varphi_1(\eta) \mu^{qp} \leq \delta - \varphi_1(\eta) \mu^{imp}, \quad (\text{CLF})$$

$$\mu^{qp} \leq \mu_{MAX}^{qp}, \quad (\text{Max QP Torque})$$

$$-\mu^{qp} \leq \mu_{MIN}^{qp}, \quad (\text{Min QP Torque})$$

$$\mu^{qp} \leq \mu_{MAX} - \mu^{imp}, \quad (\text{Max Input Torque})$$

$$-\mu^{qp} \leq \mu_{MAX} + \mu^{imp}. \quad (\text{Min Input Torque})$$

By adding the impedance control as a feed-forward term into the input torque, the model independent dynamic system (15) gathers proper information about the system. It can, therefore, adjust μ^{qp} accordingly to accommodate for the feed-forward term to achieve good tracking. By setting the

QP torque bounds μ_{MAX}^{qp} , problems with overshoot will be eliminated. We also set the total input torque bounds for the QP problem such that the final optimal input torques (22) will satisfy the hardware torque bounds μ_{MAX} and allow the control to be implemented practically on the robots or prosthetic devices.

Remark. In order to make the MIQP controller work properly, there are three parameters to be determined, which are ϵ , p and the torque bounds $\mu_{MAX}^{qp}, \mu_{MAX}$. Specifically, ϵ determines the outputs convergence rate; p is the CLF penalty term that regulates the wellness of the tracking performance and $\mu_{MAX}^{qp}, \mu_{MAX}$ are defined based on the hardware limitation. If ϵ or p are increased (corresponding to quicker convergence and heavier penalty for bad tracking), the controller will attempt to more closely match the desired trajectories but may begin to violate μ_{MAX}^{qp} due to increased torque demands, causing the QP to fail. More detailed discussion about the feasibility of the QP can be referred to [37]. To summarize, the unique merit of the MIQP controller is that it only requires the output error as the input and stabilizes the output dynamics in a rapidly exponentially convergent manner. As a result, given that μ_{MAX}^{qp} is sufficiently large, the MIQP controller will maintain the ability to adapt to systems with unknown parameters.

4 VERIFICATION ON AMBER

Before implementing the optimization-based controller on a prosthetic device with an amputee subject, the controller is verified on the bipedal robot AMBER in both simulation and experiment. The results are discussed in this section.

4.1 AMBER Test Platform

AMBER is a planar bipedal robot with 5 links (one torso, two thighs and two calves, see Fig. 4). AMBER is powered by four DC motors and is underactuated at the ankle due to a point-foot interaction with the ground. In previous work, AMBER has achieved stable and human-like walking experimentally using a proportional voltage controller [38]. In this work, we use AMBER as the platform to test the proposed prosthetic controller. The right calf is assumed to be the “prosthetic device” which has the same length and mass configuration of the left calf that is marked as the “healthy leg”. The proposed controller will be implemented on the prosthetic device, i.e., on the right knee joint. The controller for the remaining actuators will still be the original voltage controller discussed in [38].

The configuration of the AMBER model is pictured in Fig. 4 and given by the coordinates $\theta = (\theta_{sa}, \theta_{sk}, \theta_{sh}, \theta_{nsh}, \theta_{nsk})^T \in Q \subset \mathbb{R}^n$ where there are $n = 5$ coordinates and Q is the configuration space of the robot (viewed as a subset

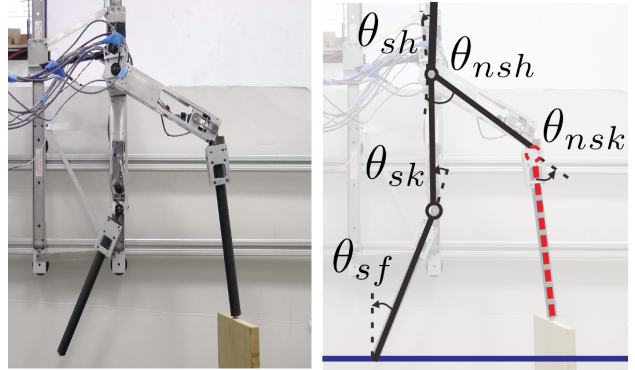


Fig. 4: The biped robot AMBER (left) and the angle conventions (right). The right leg with red dash line denotes the prosthetic device; the red dash circle represents the prosthesis joint that will be controlled using prosthetic controllers.

of \mathbb{R}^n). With the mass and length properties corresponding to the physical robot AMBER, the equations of motion for the robot can be obtained with equation (3). Note that, since AMBER has DC motors with small inductances, the electromechanical system with voltage inputs have the following form:

$$V_{in} = R_a i_a + K_\omega \omega, \quad (24)$$

where $V_{in} \in \mathbb{R}^{4 \times 1}$ is the vector of voltage inputs to the motors, $i_a \in \mathbb{R}^{4 \times 1}$ is the vector of currents through the motors, $R_a \in \mathbb{R}^{4 \times 4}$ is the resistance matrix, and $\omega \in \mathbb{R}^{4 \times 1}$ is the vector of motor speed which has the relation as $\omega = r_m \dot{\theta}$ with $r_m \in \mathbb{R}^{4 \times 4}$ denoting the total reduction of the system. Since the motors are controlled individually, with the torque constant $K_\phi \in \mathbb{R}^{4 \times 4}$, the applied inputs are:

$$u = K_\phi R_a^{-1} (V_{in} - K_\omega \omega). \quad (25)$$

Therefore, the impedance torque and QP torque discussed in Sec. 3 will be replaced with impedance voltage V^{imp} and QP voltage V^{qp} , respectively [16].

4.2 Simulation Verification with AMBER

With the model in hand, the robotic gait can be obtained using the optimization problem as discussed in Sec. 2.2 with outputs specific to the model of AMBER [16]. The simulation results of AMBER are then discussed. Tracking performance of various controllers on the joints of the prosthesis are compared. Robustness tests are also performed and compared for various controllers.

4.2.1 Tracking Performance with Different Controllers

With the exception of the prosthesis joint, on which different controllers will be implemented, the remaining joints will be

controlled with the propotional voltage control. Three different controllers are tested as the prosthetic controller: proportional control, impedance control and MIQP+Impedance control. Fig. 6 shows the tracking performances of the prosthesis knee joint using these three controllers. Using the tracking results of propotional control as the nominal reference as shown in Fig. 6a, we can see that the MIQP+Impedance control shown in Fig. 6e improves the tracking performance significantly for both stance and non-stance phases w.r.t the RMS error, while impedance control shown in Fig. 6c yields worse tracking results.

4.2.2 Stability Testing

In addition to tracking performance, the demonstration of stability and robustness are of high importance on a prosthesis controller. Two robustness tests are applied to the robot in simulation; one is to add an instantaneous push and another one is to let the robot walk above an unforeseen obstacle. In particular, a $2N$ impulse force (lasting for $0.05s$) has been applied to the prosthetic leg while in swing phase. The results show that the prosthetic device with the proposed controller can tolerate this disturbance and maintain good tracking. The same disturbance was also tested using only the impedance controller; the tracking error becomes bigger due to the disturbance and the robot falls after 6 steps. For the obstacle test, we let the robot walk over a $20mm$ high obstacle. The gait tiles of the simulation can be seen in Fig. 5,

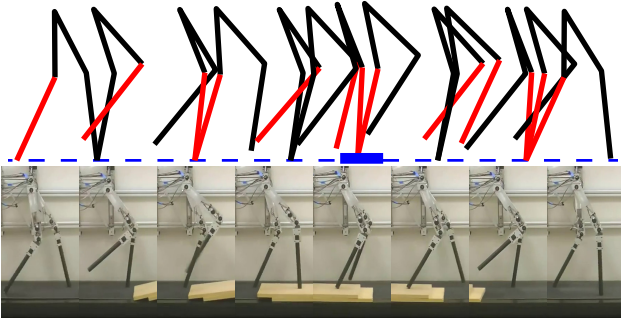


Fig. 5: Gait tiles of walking over an obstacle with MIQP+Impedance control in both simulation (top) and experiment (bottom).

Table 1: Simulation and Experiment Results Comparison of AMBER Using Different Controllers over 20 Steps.

Control	Simulation [rad]			Experiment [rad]		
	e_{rms}	e_{max}	σ_{rms}^{std}	e_{rms}	e_{max}	σ_{rms}^{std}
P	sknee	0.0155	0.0355	0.0028	0.1098	0.1563
	nsknee	0.0355	0.0738	0.0018*	0.1594	0.3823
Imped	sknee	0.0401	0.0780	0.0144	0.1060	0.1706
	nsknee	0.1403	0.3036	0.0129	0.2740	0.4770
MIQP + Imp	sknee	0.0014*	0.0109*	0.0014*	0.0355*	0.0637*
	nsknee	0.0037*	0.0220*	0.0037	0.1017*	0.2220*

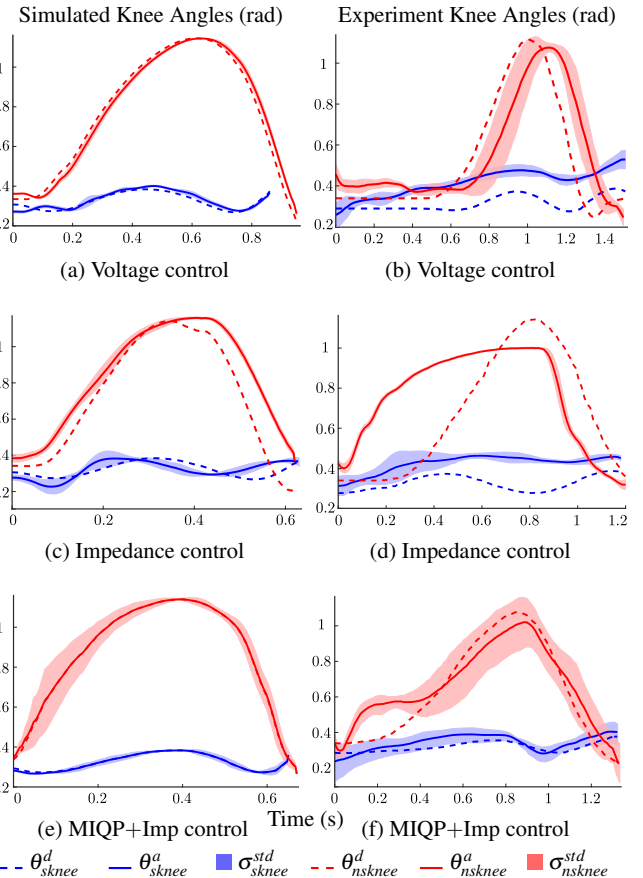


Fig. 6: The averaged actual and desired outputs of the prosthesis knee joint along with the one standard deviation over 20 steps with different controllers in both simulation (left) and experiment (right).

showing that the robot can overcome the obstacle smoothly. A similar test is also conducted with only impedance control. While the robot can walk over the obstance, tracking performance is degraded.

4.3 Experimental Verification on AMBER

Starting with the estimated impedance parameters obtained from the simulation discussed above, we are able to tune the parameters within a small range and get sustainable walking by only using the impedance controller. The tracking results of using impedance control can be seen in Fig. 6d. Compared to the tracking of propotional control as shown in Fig. 6b, the impedance control shows worse tracking performance.

MIQP+Impedance Control. Using the impedance parameters from the previous section, we apply impedance control as the feed-forward term while using the MIQP as the feedback term to correct the tracking errors and reject the disturbances. From Fig. 6f, we can see the tracking with using

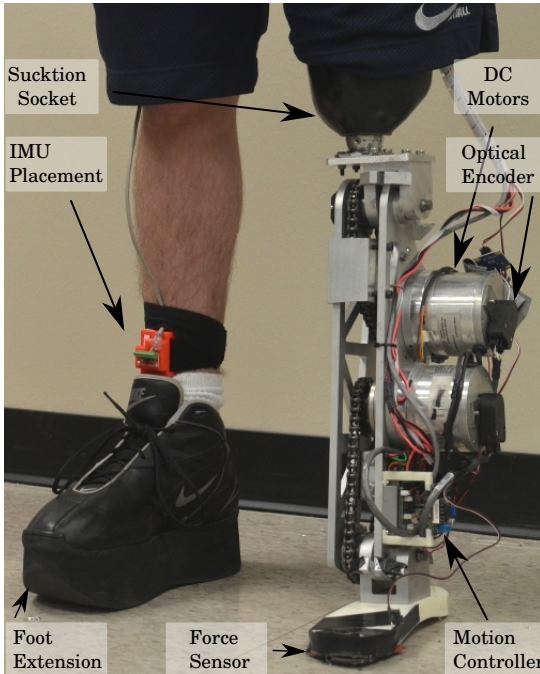


Fig. 7: Components diagram of the prosthesis AMPRO.

the MIQP+Impedance controller is the best among the three methods in both stance phase and non-stance phase (RMS error reduced by more than 50% for both phases). The detailed comparisons of both the simulation and experimental results are shown in Table. 1. One thing the readers may notice is that the MIQP+Impedance controller tends to have larger tracking variance in both the simulation and experiment, which can be seen in Fig. 6. Similar results can also be seen in Table. 1, in which the lowest one standard deviations of *rms* error are found in the tests with proportional or impedance control. Particularly, with a set of fixed controller gain, i.e., fixed control parameters, the proportional controller or impedance controller can not adjust tracking performance during the tests. On the other hand, the MIQP+Impedance controller can achieve good tracking performance in a more dynamic way even with asymmetric gaits .

Robustness of walking with MIQP+Impedance control was also tested, demonstrating the ability to overcome a 40mm block and withstand large pushes applied to the prosthetic leg. Note that, with impedance control, the robot can only overcome a 20mm block. The experiment obstacle walking gait tiles are compared with the simulated gait tiles, as shown in Fig. 5.

With the verification in both simulation and experiment as discussed above, we can conclude that the proposed optimization-based nonlinear controller shows improved tracking performance and demonstrates the ability to be more robust to disturbances and obstacles than the traditional approaches.

5 PROSTHETIC DEVICE IMPLEMENTATION

With the systematic methodology including gait generation and controller implementation verified on the robot platform, we now have the framework to realize the real-time optimization based nonlinear controller experimentally on a self-contained transfemoral prosthesis: AMPRO. The experiment setup including the design of the prosthesis AMPRO and the test subject is introduced first. Then the results of using the MIQP+Impedance controller along with other controllers are analyzed in a comparative study.

5.1 Experiment Setup

The experiment setup including the prosthetic device AMPRO and the amputee subject are introduced at this section. The two-level control architecture along with the IMU feedback sensing are also explained.

5.1.1 AMPRO

AMPRO is designed to be a high powered, compact and structurally safe device. The device uses a roller chain drive train consisting of a 374 W brushless DC motor (Moog BN34 silencer series) and a harmonic gearhead to actuate the ankle and knee joints in the sagittal plane. This design utilizes two incremental encoders for each motor and is designed to incorporate absolute encoders at the joints. Two ELMO motion controllers are used for low-level torque control purposes. Additionally, two FlexiForce (Parallax 30056) force sensors are located at the base of the foot (mounted at the toe and heel) to measure the normal reaction forces which are used for the purpose of leg switch. The prosthetic device is powered by a 8-cell LiPo battery with 4000 mAh capacity. The technical diagram can be seen in Fig. 7 and the design specifications are listed in Table. 2.

Table 2: Specifications of the AMPRO and the Subject.

Specifications	AMPRO	Amputee Subject
Total Weight (Kg)	8.1	62
Total Height (cm)	56.3	173
Socket Length (cm)	8.8	*
Calf Height (cm)	40.7	41.6
Foot Height (cm)	6.8	9
Shoe Extension (cm)	*	5.7
Ankle Range of Movement(deg)	-20 ~ 30	*
Knee Range of Movement(deg)	0 ~ 70	*
Max Joint Velocity (rpm)	81.25	*

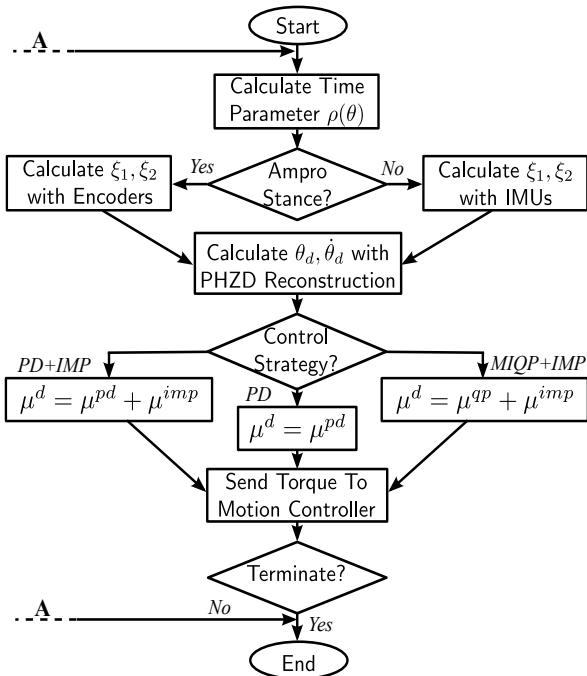


Fig. 8: Flow chart of the pseudo-code.

5.1.2 Test Subject

The experimental subject in this study has been a unilateral amputee of three years due to osteosarcoma. The subject is a 19-year-old male that utilizes a passive knee prosthesis (Ossur Total Knee 2100) for daily-use paired with a Ossur K2 Sensation foot. For the conducted experiments, the test subject's daily-use suction socket was connected to AMPRO using a standard pyramid connector. Some of the important parameters for the test subject were measured and are located in Table 2. The residual limb of the subject was measured from the approximate location of the lateral condyle to the true ankle joint and from the true ankle joint to the base of the foot (for the calf and foot measurements respectively). During the experimental trials, the test subject used a custom made shoe that features a small extension of the sole of the shoe. This extension was required in order to have the subject's residual limb of equal length to the combination of AMPRO and the subject's suction socket connection.

5.1.3 Control Architecture

The architecture of the control implementation consists a high-level controller and a low-level controller. The high-level controller of AMPRO is coded into C++ packages and runs on the Robot Operating System (ROS). The complete code is realized independently with a low-power single-board computer: Beaglebone Black (BBB) at 200 Hz. The pseudo-code of the algorithm is shown as the flowchart in Fig. 8. To provide a point of human-robotic interaction, two IMUs are

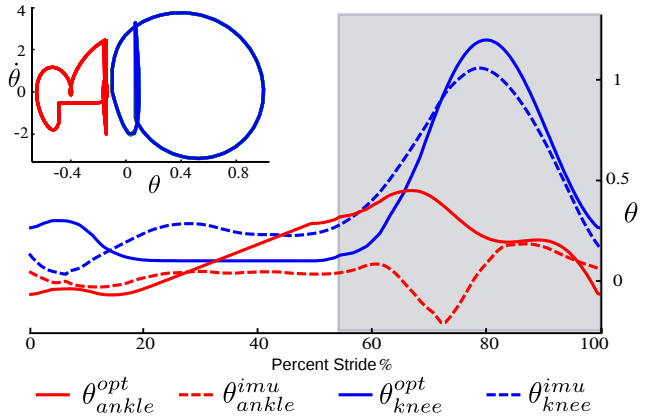


Fig. 9: Limit cycles for both the ankle and knee joints of flat-footed walking (upper left) and the comparison between the collected healthy human flat-foot walking data (IMU) and the joint angles optimized via (HIO); the shadowed region represents the swing phase.

mounted on the shin and thigh of the human leg. As the IMU sensing is used only during human stance, an IMU on the human foot is eliminated based on the assumption that the user will walk with flat-foot during the interval of interest. The EKF internal model for each IMU is used to obtain relative orientation and velocity for both the knee and ankle. In particular, while the human leg is in stance, IMU readings are utilized to compute the forward hip position ξ_1 and forward hip velocity ξ_2 . The desired swing trajectories of the prosthetic can then be calculated accordingly using the PHZD reconstruction method discussed previously. For hardware implementation, one BBB is dedicated to run the EKF algorithms as introduced in Sec. 2.2. The communication to the main BBB which runs the primary code is achieved over a networked crossover cable.

5.2 Prosthetic Gait Generation

An obvious problem encountered when designing a gait for an amputee is the lack of original locomotion data for the amputee. Human gait researchers and biomechanists have found that humans share a common pattern of joint trajectories during locomotion [23]. Therefore, a feasible approach is to use the nominal trajectories obtained from healthy subjects as the initial test gait for the amputee. While this is a common practice for prosthesis researchers and clinical physicians [10,39], this approach requires hand tuning and heuristic experience, which can be costly and time consuming. In this work, the authors propose a different approach by using the human-inspired optimization problem to design an optimized gait for the amputee, eliminating the requirement of hand tuning.

In particular, the IMU motion capture system discussed in Sec. 2.2 is utilized to collect the flat-foot trajectory of a healthy subject who has similar anthropomorphic parameters (limb lengths and body weight) of the amputee subject considered in this work. Using this trajectory set as the reference, and subject to both the PHZD constraints and physical constraints, the human-inspired optimization problem is leveraged to design a stable gait for the specific amputee subject. Note that, in the context of bipedal walking, a mathematically stable limit cycle implies stable walking. The limit cycles pictured in Fig. 9 are closed, indicating that they result in stable walking. The optimized trajectories along with the IMU motion capture data are also shown in Fig. 9. We can see that the optimized knee angle follows a similar pattern as the healthy subject. However, the optimized ankle angle is different from the reference human trajectory especially in the late stance and swing phase. This mismatch is mainly due to the flat-foot walking assumption considered in this preliminary work. This assumption constrains the reference subject to walk cautiously with a flatter ankle pattern, while on the other hand, the optimization problem could achieve a faster walking speed with more dynamic ankle trajectory.

Remark. Flat-foot walking is a simplification of human walking. We realize that it introduces limitations on both the procedure of reference trajectory recording and the prosthetic gait optimization problem. However, it captures the essential behavior of human walking that suits the preliminary testing purposes and the capabilities of the first iteration of the prosthetic device AMPRO. More complex behaviors such as multi-contact gaits will be addressed in the ongoing development of the next iteration of AMPRO which will also translate the control framework from the multi-contact capable bipedal robot, AMBER2.

5.3 Experimental Results

Before the implementation of MIQP+Impedance control on the prosthesis, a proportional-derivative (PD) controller:

$$\mu^{pd} = -K_p(\theta_a - \theta_d(\xi_1)) - K_d(\dot{\theta}_a - \dot{\theta}_d(\xi_1, \xi_2)), \quad (26)$$

is first realized to track the designed trajectories to achieve stable walking. The PD gains are tuned based on the feedback from the test subject. Walking trials were performed on a treadmill providing a constant speed of 1.3 mph. With the experimental data of walking with PD control in hand, the impedance parameters are estimated using the least-square-error fitting method. We then apply impedance control as the feed-forward term while using the MIQP control as the feedback term to track the desired joint trajectories. In particular, for the first round of testing, we set both the torque bounds μ_{MAX}^{qp} and μ_{MAX} to be 40 Nm which is determined

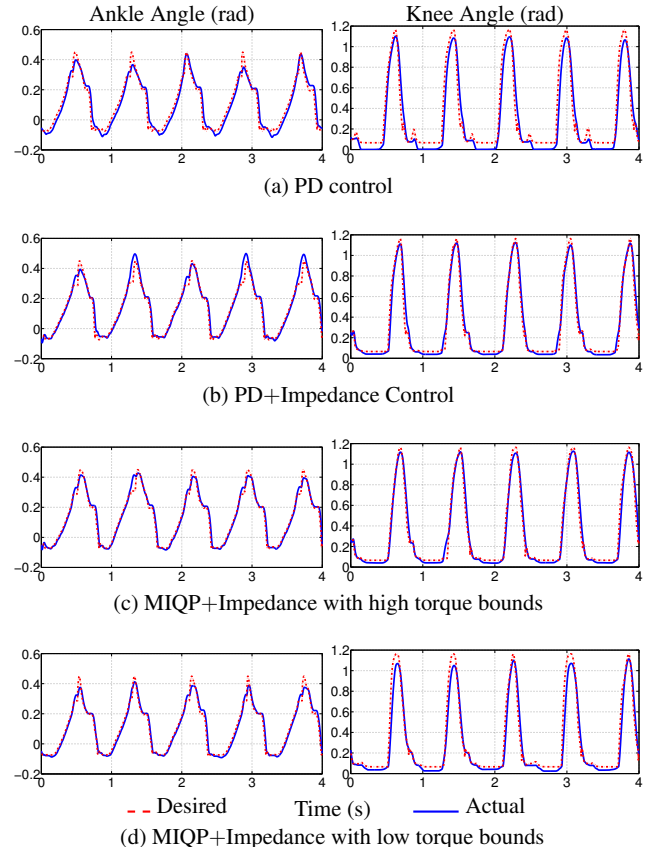


Fig. 10: Tracking comparison for different controllers.

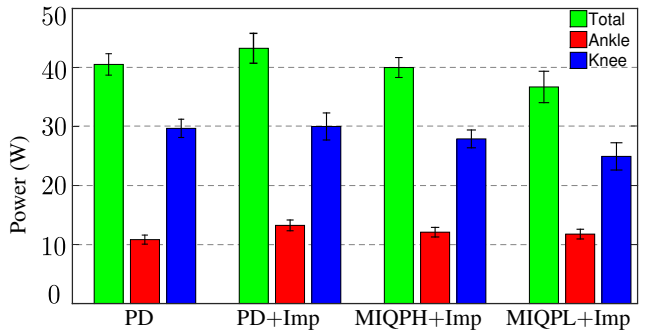


Fig. 11: Net mechanical power comparison for the prosthetic joints of one step (including stance phase and swing phase) averaged over 32 steps with using different controllers.

based on the PD walking experiment data. In order to show the torque optimality of the proposed novel controller, the torque bounds μ_{MAX}^{qp} and μ_{MAX} are reduced to be 20 Nm for the second round of testing. While the novel control contains both the feedback term and feed-forward term, we also compare it with an augmented control strategy, PD+Impedance:

$$\mu^d = \mu^{pd} + \mu^{imp}, \quad (27)$$

which also includes impedance control as a feed-forward term. In order to show the tracking performance visually, the tracking results of five consecutive steps using different

controllers are plotted in a comparative way in Fig. 10. For further statistical verification purposes, a total of 32 steps are considered to compute the performance results for each of the considered controllers. In particular, the averaged one step mechanical power consumption along with the corresponding one standard deviation of the prosthetic device is shown in Fig. 11. More detailed performance comparisons are listed in the Table. 3. The gait tiles of the level walking using the proposed optimization-based controller along with the simulated gaits are shown in Fig. 12.

5.4 Discussion

A joint tracking comparison is provided in Fig. 10 for various controllers on the knee and ankle joints of AMPRO. It is evident that the tracking performance of both the ankle and the knee are exceptionally good for MIQP+Impedance control. The tracking results with lower torque bounds are shown in Fig. 10d. While the tracking performance is not as good as the tracking with higher torque bounds, it is better than using PD control, with a 20.9% improvement on *rms* error based over 32 steps. More importantly, this improved tracking is achieved with lower torque and less total energy consumption when compared to PD control (9.4% improvement). Similar performance can also be found of MIQPH+Impedance control when comparing to PD+Impedance control with less than 5% tracking loss but 3.26W (7.5%) reduction on power, which can be seen in Fig. 11 and Table. 3.

To illustrate the overall control performance more clearly, the experimental results (including tracking errors, maximum torque requirement and average net power consumption) of 32 consecutive steps are listed in Table. 3. In particular, the best performances are highlighted in the table with a * superscript, from which we can see that with the exception of the *rms* knee error (using PD+Impedance) and the minimum ankle power (using PD control), all of the best performances are achieved with the MIQP+Impedance controllers. The low power requirements of the PD controlled ankle are also correlated with the highest tracking errors,

Table 3: Experiment Results Comparison of AMPRO Using Different Controllers over 32 Steps.

Control	e_{rms}	e_{max}	σ_{rms}^{std}	$\tau_{max}[Nm]$	$P[W]$
PD	Ankle	0.0388	0.1700	0.0027*	24.749
	Knee	0.1059	0.3957	0.0179	41.275
PD+ Imp	Ankle	0.0325	0.1860	0.0070	23.787
	Knee	0.0546*	0.3693	0.0148	38.921
MIQPL +Imp	Ankle	0.0290	0.1290*	0.0033	19.916*
	Knee	0.0854	0.3822	0.0155*	20.027*
MIQPH +Imp	Ankle	0.0261*	0.1498	0.0045	22.351
	Knee	0.0657	0.3002*	0.0213	36.221
					27.902

indicating that low fidelity tracking performance may be allowing passive motion of the device. To summarize, the experimental results indicate that the MIQP+Impedance controller has the most balanced performance between tracking and power requirements.

The resulting powered prosthetic joint trajectories using the proposed optimization-based controller and the PD controller are compared with the IMUs collected healthy human locomotion data and the passive prosthetic walking data (the amputee walking with a passive device) in Fig. 13. When compared to passive prosthetic walking, we can see that the ankle movement of the powered device is much more dynamic than that of the passive device. In particular, the ankle on the passive device is very rigid and possesses a very small movement range. On the other hand, the powered prosthetic ankle can provide a more dynamic panarflexion throughout the stance phase and dorsiflexion during the swing phase. The human-likeness of the ankle joint will be improved in the future work with multi-contact walking. For the knee joint, we can see that both the passive device and powered device with different controllers have a similar swing pattern compared to the healthy human walking. However, for the stance knee trajectory, both the passive device and the powered device with PD control tend to lock the knee at the last portion of the stance phase. Note that, for both the passive device and powered device, a safety stop is added at the knee joint to prevent hyper-extension, where we define as knee-lock if the knee joint reaches this position. During data collecting, we calibrate this knee-lock position as zero reference point in particular. Alternatively, the powered device with MIQP+Impedance control has better performance with bigger knee bending and no knee locking. A slight delay was also noticed for the powered prosthetic walking when switching from stance phase to swing phase. This was caused by the delay of the force sensor recovering from the loaded status during the stance phase, which will be fixed by considering a load cell in the future design.

6 CONCLUSIONS

This work proposed a novel systematic methodology, including gait generation and optimization-based control, to achieve prosthetic walking for any specific subject, while at the same time aiming to improve control optimality and reduce clinical tuning. In particular, benefiting from the low-cost IMU motion capture system and the human-inspired optimization problem, a smooth and locally optimal prosthetic gait can be designed specifically for the amputee while simultaneously being applicable to the prosthetic device. The real-time optimization based nonlinear controller (MIQP+Impedance) shows improved performance with respect to both tracking and energy efficiency. This methodology was first validated on the bipedal robotic platform, then implemented

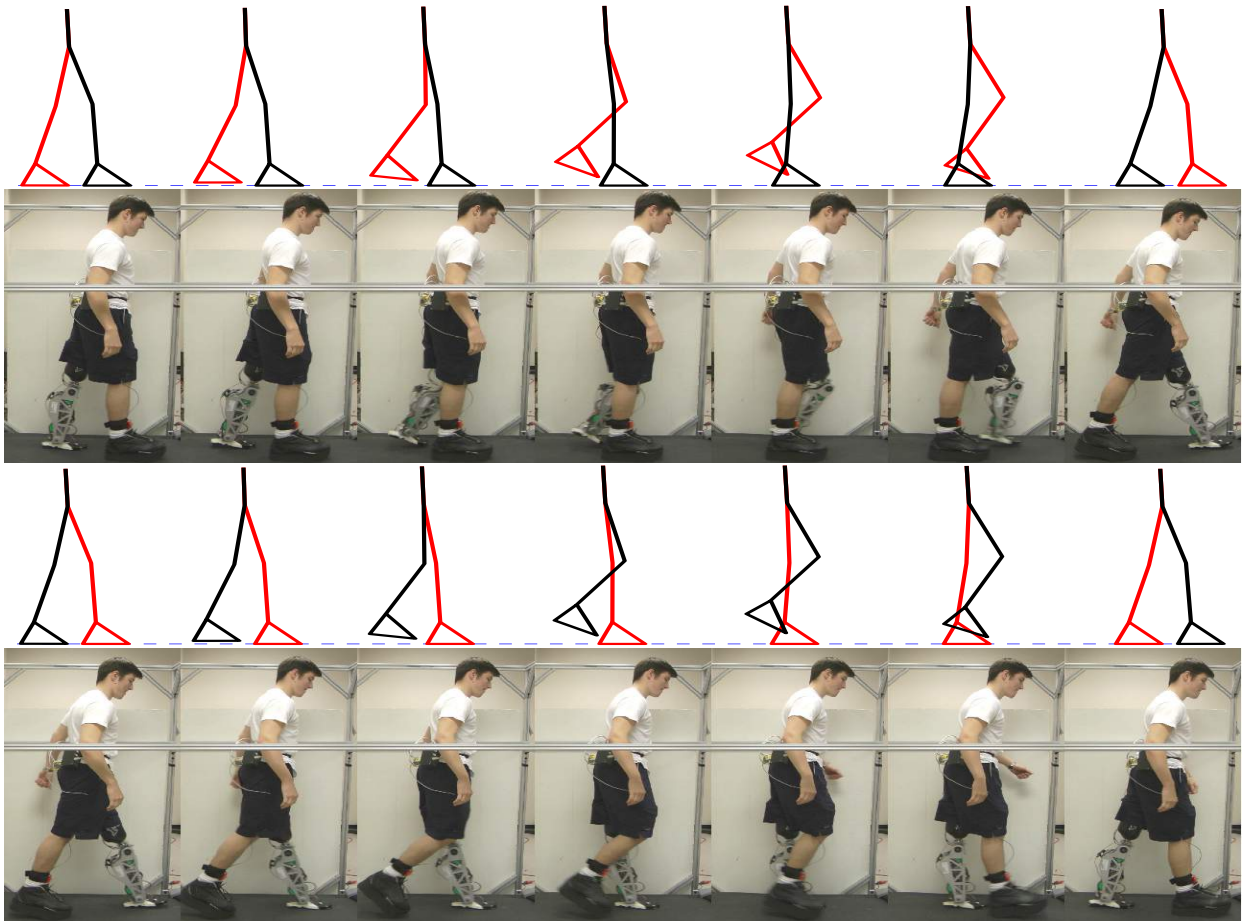


Fig. 12: Gait tile comparison between the outside NHS experimental walking and the simulated walking.

on the self-contained transfemoral prosthesis AMPRO to achieve stable prosthetic walking with an amputee.

Traditional control approaches (e.g. variable impedance control) to powered prostheses rely on the extensive use of many control parameters in order to achieve successful operation of the device or for a particular subject. The methodology in this work takes the first steps toward designing the controllers and verifying their application both in simulation and on the bipedal robot platform before implementation on a prosthetic device. Benefiting from this formal approach, it has the potential to reduce clinical testing and tuning for the amputee at the gait and control design stage. While future work should focus on showing that this approach also helps on the adaptation and comfortability of amputees, we believe that with the automation of the gait generation and controller design process proposed in this work, the tuning can potentially be reduced and the adaptation can be achieved in a more intuitive way. A new 3D-capable AMPRO prosthesis is currently being designed with two serial-elastic-actuator (SEA) powered pitch joints in the sagittal plane and a passive compliant ankle roll joint in the coronal plane. The new design is also focused on reducing

the size of the electric motors, optimizing other structural components and adding load cells with the aim of providing a more comfortable experience for the user while reducing overall power consumption. Future work will be also focused on the realization of a multi-contact walking gaits (as realized on bipedal robot AMBER2 in [31]) and different locomotion modes on the new device to achieve more natural and versatile human-like prosthetic walking.

Acknowledgment

This research is supported under: NSF CAREER Award CN-S-0953823 and Texas Emerging Technology Fund 11062013. This research has approval from the Institutional Review Board from Texas A&M University with IRB2014-0382F for testing with human subjects.

References

1. T. Dillingham. Limb amputation and limb deficiency: Epidemiology and recent trends in the united states. *Southern Medical Journal*, 2002.

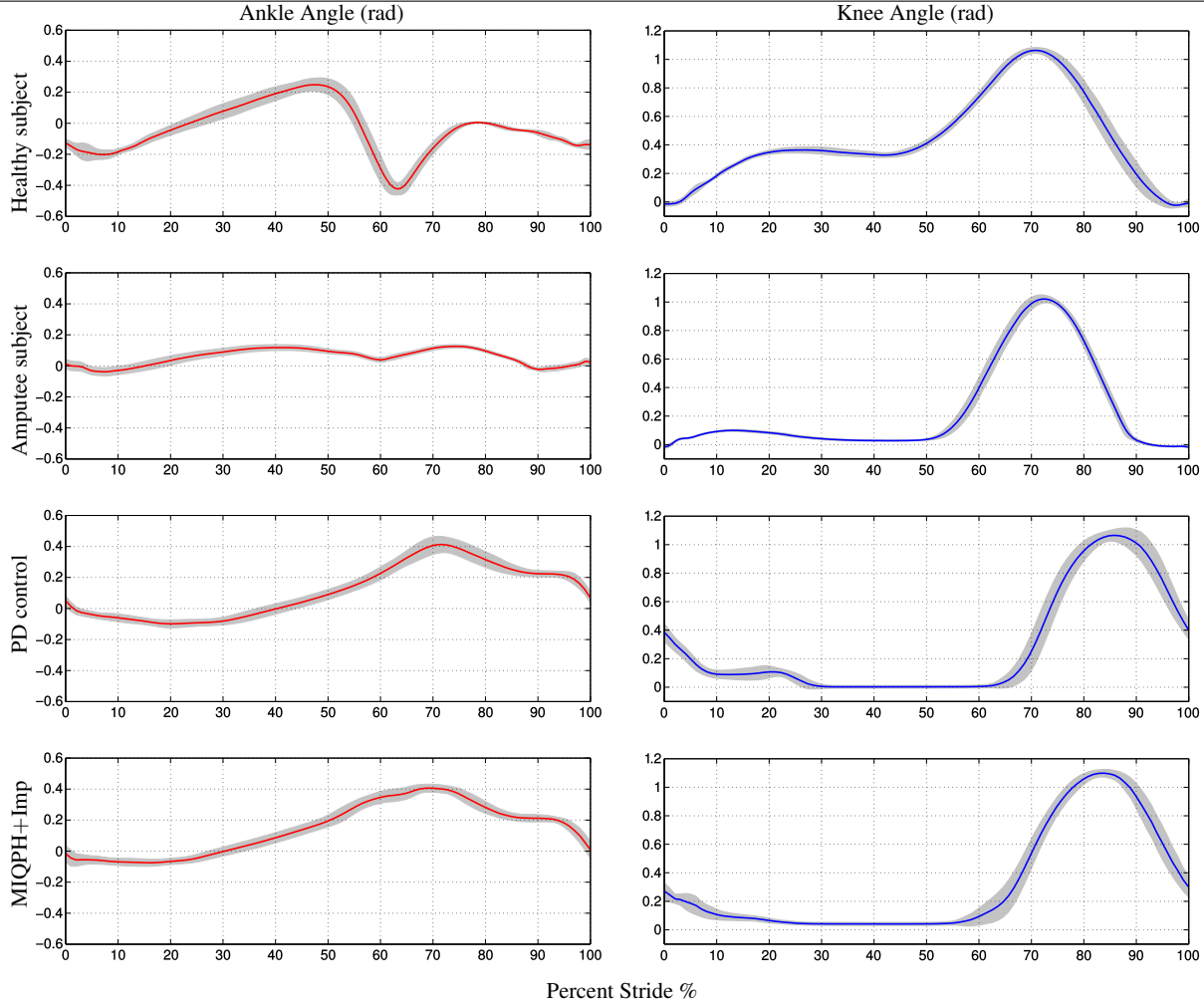


Fig. 13: Comparisons of both the ankle and knee joint angles of healthy human walking, passive prosthetic walking and powered prosthetic walking with PD control and MIQPH+Impedance control. The gray area represents one standard deviation of each corresponding trajectory for 32 steps.

2. D. Winter. *The Biomechanics and Motor Control of Human Gait: Normal, Elderly, and Pathological*. University of Waterloo Press, 1991.
3. W. Flowers and Mann. Electrohydraulic knee-torque controller for a prosthesis simulator. *ASME J. of Biomechanical Engineering*, 99(4):3–8, 1977.
4. D. Grimes, W. Flowers, and M. Donath. Feasibility of an active control scheme for above knee prostheses. *ASME J. of Biomechanical Engineering*, 99(4):215–221, 1977.
5. J. Hitt, A. M. Oymagil, T. Sugar, K. Hollander, A. Boehler, and J. Fleeger. Dynamically controlled ankle-foot orthosis (dco) with regenerative kinetics: incrementally attaining user portability. In *Robotics and Automation, 2007 IEEE International Conference on*, pages 1541–1546.
6. A. M. Oymagil, J. K. Hitt, T. Sugar, and J. Fleeger. Control of a regenerative braking powered ankle foot orthosis. In *Rehabilitation Robotics, 2007. IEEE 10th International Conference on*, pages 28–34.
7. R. Rarick, H. Richter, A. van den Bogert, D. Simon, H. Warner, and T. Barto. Optimal design of a transfemoral prosthesis with energy storage and regeneration. In *American Control Conference*, pages 4108–4113, June 2014.
8. R. Gregg, T. Lenzi, L. Hargrove, and J. Sensinger. Virtual constraint control of a powered prosthetic leg: From simulation to ex-

- periments with transfemoral amputees. *Robotics, IEEE Transactions on*, 30(6):1455–1471, Dec 2014.
9. S. Au, M. Berniker, and H. Herr. Powered ankle-foot prosthesis to assist level-ground and stair-descent gaits. *Neural Networks*, 21(4):654 – 666, 2008.
10. F. Sup, A. Bohara, and M. Goldfarb. Design and Control of a Powered Transfemoral Prosthesis. *The International journal of robotics research*, 27(2):263–273, Feb. 2008.
11. A. Boehler, K. Hollander, T. Sugar, and D. Shin. Design, implementation and test results of a robust control method for a powered ankle foot orthosis (afo). In *Robotics and Automation, 2008 IEEE International Conference on*, pages 2025–2030.
12. K. Hollander and T. Sugar. A robust control concept for robotic ankle gait assistance. In *Rehabilitation Robotics, 2007 IEEE 10th International Conference on*, pages 119–123.
13. J. A. Blaya and H. Herr. Adaptive control of a variable-impedance ankle-foot orthosis to assist drop-foot gait. *Neural Systems and Rehabilitation Engineering, IEEE Transactions on*, 12(1):24–31, 2004.
14. N. Fey, A. Simon, A. Young, and L. Hargrove. Controlling knee swing initiation and ankle plantarflexion with an active prosthesis on level and inclined surfaces at variable walking speeds. *Translational Engineering in Health and Medicine, IEEE Journal of*, 2:1–12, 2014.

15. H. Zhao and A. D. Ames. Quadratic program based control of fully-actuated transfemoral prosthesis for flat-ground and up-slope locomotion. *IEEE, American Control Conference*, pages 4101 – 4107, 2014.
16. H. Zhao, S. Kolathaya, and A. D. Ames. Quadratic programming and impedance control for transfemoral prosthesis. *Robotic and Automation, 2014 IEEE, International Conference on*, pages 1341 – 1347.
17. H. J. Luinge and P. H. Veltink. Measuring orientation of human body segments using miniature gyroscopes and accelerometers. *Medical and Biological Engineering and computing*, 43(2):273–282, 2005.
18. D. Roetenberg, H. Luinge, and P. Slycke. Xsens mvn: full 6dof human motion tracking using miniature inertial sensors. *Xsens Motion Technologies BV, Tech. Rep.*, 2009.
19. N. Miller, O. C. Jenkins, M. Kallmann, and M. J. Mataric. Motion capture from inertial sensing for untethered humanoid teleoperation. In *Humanoid Robots, 2004 IEEE/RAS 4th International Conference on*, volume 2, pages 547–565.
20. S. Šlajpah, R. Kamnik, and M. Munih. Kinematics based sensory fusion for wearable motion assessment in human walking. *Computer methods and programs in biomedicine*, 116:131–144, 2013.
21. H. Zhao, M. Powell, and A. D. Ames. Human-inspired motion primitives and transitions for bipedal robotic locomotion in diverse terrain. *Optimal Control Applications and Methods*, 35:730–755, 2013.
22. S. Jiang, S. Partrick, H. Zhao, and A. Ames. Outputs of human walking for bipedal robotic controller design. In *American Control Conference (ACC), 2012*, pages 4843–4848, 2012.
23. D. Winter. *Biomechanics and Motor Control of Human Movement*. Wiley-Interscience, New York, 2 edition, 1990.
24. A. Ames. Human-inspired control of bipedal walking robots. *Automatic Control, IEEE Transactions on*, 59:1115 – 30, 2012.
25. S. Sastry. *Nonlinear Systems: Analysis, Stability and Control*. Springer, New York, 1999.
26. A. Ames. First steps toward automatically generating bipedal robotic walking from human data. *Robotic Motion and Control*, 422:89–116, 2012.
27. Y. Hürmüzlü and D. Marghitu. Rigid body collisions of planar kinematic chains with multiple contact points. *Intl. J. of Robotics Research*, 13(1):82–92, 1994.
28. E. Westervelt, J. Grizzle, C. Chevallereau, J. Choi, and B. Morris. *Feedback Control of Dynamic Bipedal Robot Locomotion*. CRC Press, 2007.
29. A. Ames, R. Vasudevan, and R. Bajcsy. Human-data based cost of bipedal robotic walking. In *Hybrid Systems: Computation and Control*, pages 153–162, Chicago, IL, 2011.
30. W.-L. Ma, H. Zhao, S. Kolathaya, and A. D. Ames. Human-inspired walking via unified pd and impedance control. In *Robotic and Automation, 2014 IEEE International Conference on*, pages 5088 – 5094.
31. H. Zhao, W.-L. Ma, M. B. Zeagler, and A. D. Ames. Human-inspired multi-contact locomotion with AMBER2. In *Cyber Physics System, 2014 IEEE International Conference on*, pages 199–210.
32. A. Ames, K. Galloway, and J. Grizzle. Control lyapunov functions and hybrid zero dynamics. In *Decision and Control (CDC), 2012 IEEE 51st Annual Conference on*, pages 6837–6842.
33. N. Hogan. Impedance control: An approach to manipulation. pages 304–313, 1984.
34. N. Aghasadeghi, H. Zhao, L. J. Hargrove, A. D. Ames, E. J. Perreault, and T. Bretl. Learning impedance controller parameters for lower-limb prostheses. *Intelligent Robots and Systems, 2013 IEEE/RSJ International Conference on*, pages 4268–4274.
35. D. Atherton and S. Majhi. Limitations of pid controllers. In *American Control Conference*, pages 3843–3847, 1999.
36. A. D. Ames, K. Galloway, J. Grizzle, and K. Sreenath. Rapidly exponentially stabilizing control lyapunov functions and hybrid zero dynamics. *IEEE Trans. Automatic Control*, 59:876–891, 2014.
37. B. Morris, M. Powell, and A. Ames. Sufficient conditions for the lipschitz continuity of qp-based multi-objective control of humanoid robots. In *Decision and Control (CDC), 2013 IEEE 52nd Annual Conference on*, pages 2920–2926.
38. S. N. Yadukumar, M. Pasupuleti, and A. Ames. Human-inspired underactuated bipedal robotic walking with AMBER on flat-ground, up-slope and uneven terrain. In *Intelligent Robots and Systems, 2012 IEEE International Conference on*, pages 2478–83, Portugal.
39. J. W. H. Herr and S. Au. Powered ankle-foot prosthesis. *Biomechanics of the Lower Limb in Health, Disease and Rehabilitation*, pages 72–74, 2007.